Molecular dynamics investigation of structural properties of a zeolite ZSM-5 based amorphous material

A. B. Mukhopadhyay*
Institut für Physikalische und Theoretische Chemie, Universität Bonn, Wegelerstrasse 12, D-53115 Bonn, Germany

C. Oligschleger
Fachhochschule Bonn–Rhein–Sieg, University of Applied Sciences, von-Liebig-Strasse 20, D-53359 Rheinbach, Germany

M. Dolg
Institut für Theoretische Chemie, Universität zu Köln, Greinstrasse 4, D-50939 Köln, Germany
(Received 19 August 2002; published 23 January 2003)

Results of molecular dynamics simulations on structural properties of zeolite ZSM-5 based amorphous solids are presented. The topology of the network is analyzed by pair-distribution functions, bond angle distributions, and coordination number distribution. The effects of the extent of amorphization, measured by an energetic criterion, on properties like the distribution of coordination numbers, internal surface area, ring statistics, and effective pore size are studied. Analysis of the amorphized systems further reveals that due to the partial collapse of the zeolite framework, the porosity and internal surface area for large and small substrates are reduced and increased, respectively, possibly allowing a design of material with specific desired catalytic properties. Ring statistics indicates that upon amorphization not only rings with larger size break down to give rings with smaller size, but that for intermediate degree of amorphization also larger rings are generated.

DOI: 10.1103/PhysRevB.67.014106 PACS number(s): 61.43.Er, 31.15.Qg, 68.47.Gh, 82.75.Fq

I. INTRODUCTION

Zeolites are technologically an important class of materials utilized in a wide variety of industrial applications, including catalysis,[1–5] ion exchange,[6,7] back fill material for nuclear waste disposal,[8,9] and chemical sensing.[10] The study of zeolite-based amorphous materials can also be important for technological applications. Pore size and shape, Si/Al ratio, or other modifications such as extra-framework cation exchange, isomorphous substitution, pore blockage, elimination of external sites, etc., are varying parameters for determining the product selectivity of zeolitic catalysis.[2] Recently, it was shown that ZSM-5 and ferrite-based ZSM-5 materials with x-ray diffractogram (XRD) crystallinity level as low as 2% exhibited superior catalytic performance (higher selectivities and yields) in the skeletal isomerization of linear butenes to isobutenes compared to their conventional highly crystalline analog. This was attributed to be a consequence of decreased zeolite pore lengths that are presumably present in these amorphous materials.[11] Zeolites like analcime, natrolite, and zeolite-Y, when exposed to high-radiation doses and electron irradiation, undergo amorphization, which causes remarkable effects on ion exchange and sorption capacity due to the closure of structural channels.[12,13] Pressure-induced amorphization of hydrated Na-A zeolite leads to a disordered state which exhibits an unusual dependence of the conductivity on the pressure, which could be exploited in specific applications.[14] In the synthesis of certain alumino silicate-based ceramic materials, thermal transformation of the zeolite precursors is a novel route, where the reaction proceeds via amorphous intermediate phases,[15] Studies on the mechanical treatment of zeolites show that amorphization causes remarkable changes in vibrational IR spectra and XRD.[16,17] This implies that the amorphization process, i.e., the transformation from long-range to short-range ordering of the framework, is caused by structural changes at the molecular level. Thus, studies of structural aspects in these amorphous zeolite-based systems and their correlation to microscopic properties presents a fascinating challenge. Hence, understanding the dependence of physical and chemical properties on the microstructure is critical for designing new materials suitable for specific applications.

Due to the lack of translational symmetry, standard experimental methods have some limitations to derive a detailed picture of the microscopic structure and, hence, simulation techniques like molecular dynamics (MD) and Monte Carlo (MC) have become widely used tools to explore complicated amorphous systems. MC methods are applied to explore configuration space, i.e., to search for minimum-energy structures and to establish their properties as well as to study relaxation from a global point of view. However, sometimes the move classes may be unphysical and do not give reliable insight into the microscopic dynamics of the systems. MD is widely used to construct models of the amorphous state by rapid quenching of structures at high temperature and analyzing the dynamics of the model on a microscopic scale. The success of MD depends crucially on the quality of the interaction potentials used to determine the energy and the forces between interacting particles.

In the present contribution, we present results for the structural properties of amorphous forms derived from ZSM-5 using MD simulations. To the best of our knowledge, this is the first extensive theoretical investigation of ZSM-5 (or any other zeolite) based amorphous material. Our paper is organized as follows: In Sec. II we describe the interaction potential and give details of the simulations that have been carried out for the amorphization of ZSM-5 zeolite. The analysis of short-range order is given in Sec. III. The connectivity among basic elementary units is discussed in Sec.

IV. In Sec. V, the effects of the extent of amorphization on properties like coordination number distribution, internal surface area, ring distribution, and pore size are described in detail. Some concluding remarks are then given in the end.

II. COMPUTATIONAL DETAILS

Our calculations have been carried out with a modified and extended version[18] of the code of Oligschleger and Laird.[19]

A. Interaction potential

The pairwise atomic interaction potential proposed by Kramer *et al.*[20] was used in all our simulations reported here. It was parametrized using data from *ab initio* calculations and experiment for achieving high accuracy and transferability. This potential has already been sucessfully applied for modeling of crystalline zeolite systems.[21] The functional form is of the Buckingham type, given by

$$\phi(r_{\alpha\beta}) = \frac{q_\alpha q_\beta e^2}{r_{\alpha\beta}} + A_{\alpha\beta}\exp(-B_{\alpha\beta}r_{\alpha\beta}) - \frac{C_{\alpha\beta}}{r_{\alpha\beta}^6}, \quad (1)$$

where $r_{\alpha\beta}$ is the distance between the two ions α and β $(\alpha,\beta \in \{\mathrm{Si,O}\})$. The values of the partial charges q_α and q_β and the constants $A_{\alpha\beta}, B_{\alpha\beta}$, and $C_{\alpha\beta}$ are documented in Ref. 20. The cutoff radius for the short-range and long-range parts was taken to be 7.5 Å and 17.5 Å, respectively. The long-range Coulomb part was evaluated by means of Ewald summation.[22]

B. Preparation of amorphous configurations

Our simulations have been carried out on a (formally periodic) system with 3456 particles (Si,O) in the central MD box. The amorphous states of the silicious zeolite were generated by starting with an orthorhombic lattice of silicious ZSM-5, also widely known as silicalite, whose initial positional parameters were taken from Ref. 23. This initial configuration was heated to the temperatures $T=4700$ K, 4800 K, 4900 K, and 5000 K, with heating rate $D_{heat}<4.7\times10^{13}$ K/s, was then equilibrated, and finally quenched directly to $T=300$ K with quenching rate $D_{quench}<4.7\times10^{13}$ K/s, followed by equilibration and storage of atomic coordinates. Different maximum temperatures were applied in order to study the effect of the extent of amorphization on structural properties. Whereas properties such as coordination number, internal surface area, or ring and pore size distribution are affected by the extent of amorphization, i.e., the maximum temperature, the positions of the peaks of the pair correlation functions and bond angle distributions are not. Vollmayr *et al.* demonstrated by simulations of amorphous silica that microscopic properties (radial distribution function, bond angle distribution, and ring size distribution) are more affected by the choice of the quenching rate than macroscopic properties (density, enthalpy thermal expansion coefficient).[24,25] Nevertheless, the simulated results using orders of magnitude higher quenching rates than feasible in the laboratory, e.g., the positions of the peaks of the pair correlation functions and bond angle distributions, are usually in good agreement with experimental data. The number density in the simulation cell was kept constant during all MD runs and corresponds to a mass density of 1.785 g/cm^3. The equilibration was always done via constant-temperature MD simulations, by integrating the equation of motion with the velocity form of the Verlet algorithm using periodic boundary conditions. The equilibration time was about 0.6 ns corresponding to 3×10^5 integration steps. The time step was kept sufficiently small to guarantee a negligible drift of the total energy. For constant-temperature MD simulations various methods of temperature control are commonly used, i.e., velocity rescaling,[26] coupling to an external heat bath,[27] or by adding chains of fictitous heat bath particles in the so-called Nosé-Hoover dynamics.[28] We used the velocity rescaling method, where we averaged $T(t_i)$ over a period of 20 time steps $[T_{av}=\frac{1}{20}\Sigma_{i=m}^{m+19}T(t_i)]$ and scaled the velocities after each period by $\sqrt{T_0/T_{av}}$ with T_0 being the "desired" temperature and T_{av} being the averaged temperature.

We monitor the atomic displacements during the course of MD runs by

$$\Delta R(t) = \sqrt{\sum_n [\boldsymbol{R}^n(t) - \boldsymbol{R}^n(0)]^2}, \quad (2)$$

where $\boldsymbol{R}^n(t)$ is the position vector of particle n at time t and $\boldsymbol{R}^n(0)$ is the one at the starting or reference configuration. If the total displacement of the atoms exceeds a cutoff value and the residence time of the atoms in the new positions also exceeds a minimal period of at least 3 times the period of a typical soft vibrational mode, the new positions of the particles were accepted as a starting point for the determination of a possible new minimum configuration. The cutoffs of displacements and resident time are chosen to avoid spurious minima. All stored coordinates were then quenched to $T=0$ using a combined steepest-descent conjugate-gradient algorithm[29] to locate the nearest minimum configuration. These were further used for the analysis of the structural properties of the amorphous material.

III. SHORT-RANGE ORDER

In order to understand the dynamical behavior of the system it is also necessary to investigate its static properties since important aspects of its catalytic activity like diffusion of ions, atoms, and molecules are intimately related to the network of rings and pores of the system. Similarly, other dynamical properties to be dealt with in a future publication,[30] e.g., density of vibrational states, depend on the structure.

To get insight into the two-body structural correlation we have calculated total and partial pair-distribution functions from the MD trajectories. Partial pair-distribution functions $g_{\alpha\beta}$ are calculated from

$$\langle n_{\alpha\beta}(r)\rangle \Delta r = 4\pi r^2 \Delta r \rho_N c_\beta g_{\alpha\beta}(r), \quad (3)$$

where $n_{\alpha\beta}\Delta r$ is the number of particles of species β in a shell of thickness Δr and radius r around a particle of species α, and $\langle\cdots\rangle$ represents the ensemble average and aver-

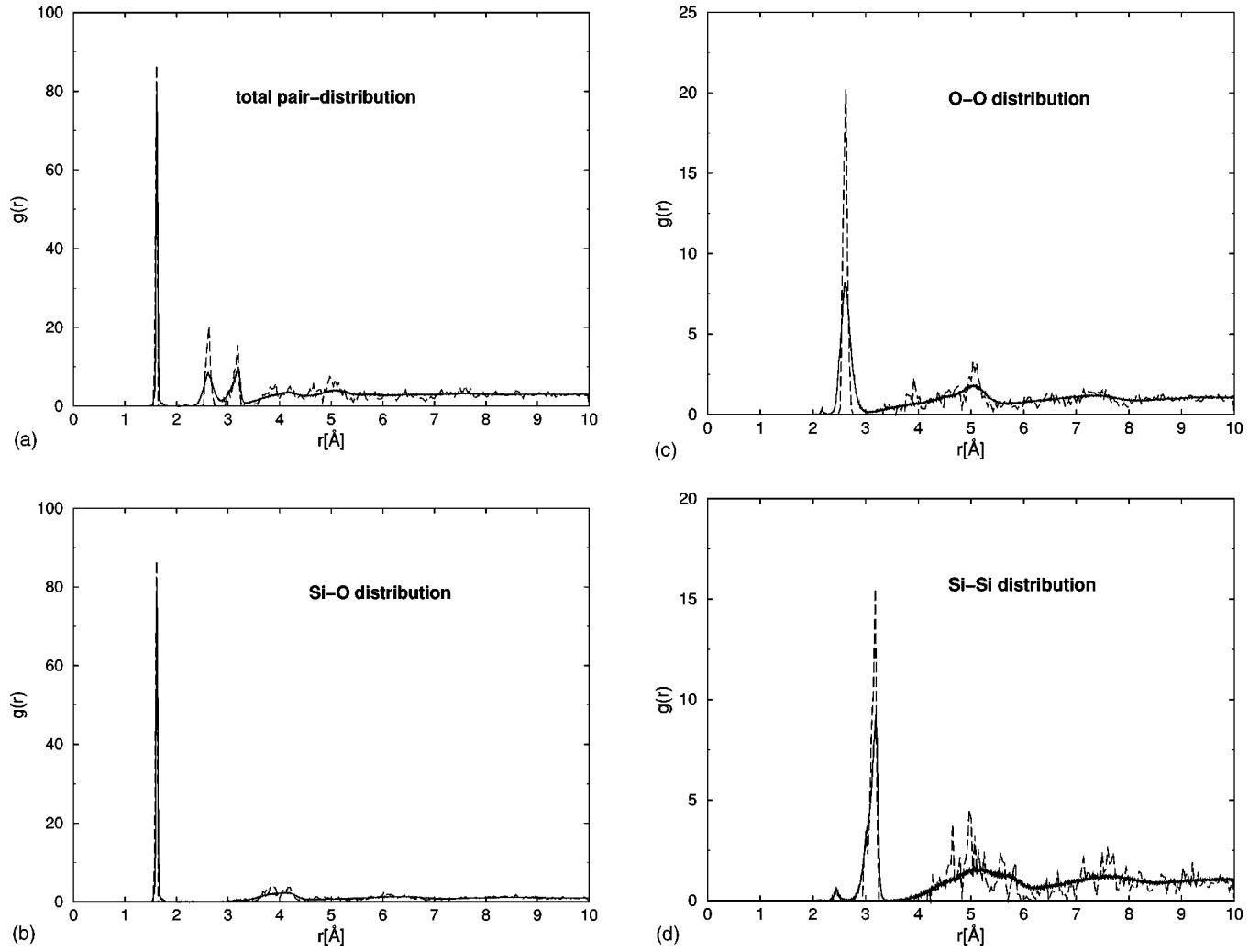

FIG. 1. Total pair-distribution function (a) and the partial pair-distribution functions (b)–(d) in amorphous zeolite (solid line) at $T = 300$ K derived from the crystalline structure (long-dashed line) when heated to 5000 K.

age over all particles of species α. ρ_N is the total number density $(N/V, N=N_\alpha+N_\beta)$ and c_β is the concentration of species β. The contributions to the total pair-distribution function can be assigned by the peaks obtained in the partial pair-distribution functions. The computed total pair-distribution function and partial pair-distribution functions of Si-O, O-O, and Si-Si are shown in Fig. 1. The most intense peak in the total pair-distribution function [Fig. 1(a)] arises from $g_{Si\text{-}O}$ [Fig. 1(b)], smaller peaks at larger distances from $g_{O\text{-}O}$ [Fig. 1(c)] and $g_{Si\text{-}Si}$ [Fig. 1(d)]. From the positions of these peaks we conclude that the Si-O bond length is 1.62 ± 0.04 Å and the nearest-neighbor O-O and Si-Si distances are 2.61 ± 0.21 Å and 3.19 ± 0.15 Å, respectively. The errors are obtained from the full width at half maximum (FWHM). The physical significance of the small peaks observed at smaller r than the most intense peaks appearing in Figs. 1(c) and 1(d) is discussed later.

The average coordination number (CN) of species α surrounded by species β, $Z_{\alpha\beta}$, is one of the most important pieces of information that can be obtained by performing integration around the first peak in the pair-distribution function:

$$Z_{\alpha\beta}(R) = 4\pi\rho_\beta \int_0^R g_{\alpha\beta}(r) r^2 dr. \tag{4}$$

Here R is the cutoff radius, usually chosen as the position of the minimum after the most intense peak of $g_{\alpha\beta}(r)$. For this integration the cutoff radii for Si-O, O-O, and Si-Si are taken as 1.8 Å, 3.1 Å, and 3.4 Å, respectively. From this analysis it is found that Si atoms are on the average coordinated by 3.99 O atoms and surrounded by 3.95 Si atoms. Similarly O atoms are coordinated by 2.00 Si atoms and surrounded by 6.02 O atoms. These findings indicate that the most common structural feature are all corner-sharing SiO_4 tetrahedra. The deviations from this pattern are discussed below.

The three-body correlations in amorphous ZSM-5 based material are examined and compared to the crystalline ZSM-5 through bond angle distributions plotted in Fig. 2, which give further information on local structural units. The O-Si-O angle distribution has the main peak at 108° with FWHM of 12.6°. The O-O-O angle distribution has an intense sharp peak at 59.4° with FWHM of 7.2° and the O-O-Si angle distribution has a main peak at 35.1° with

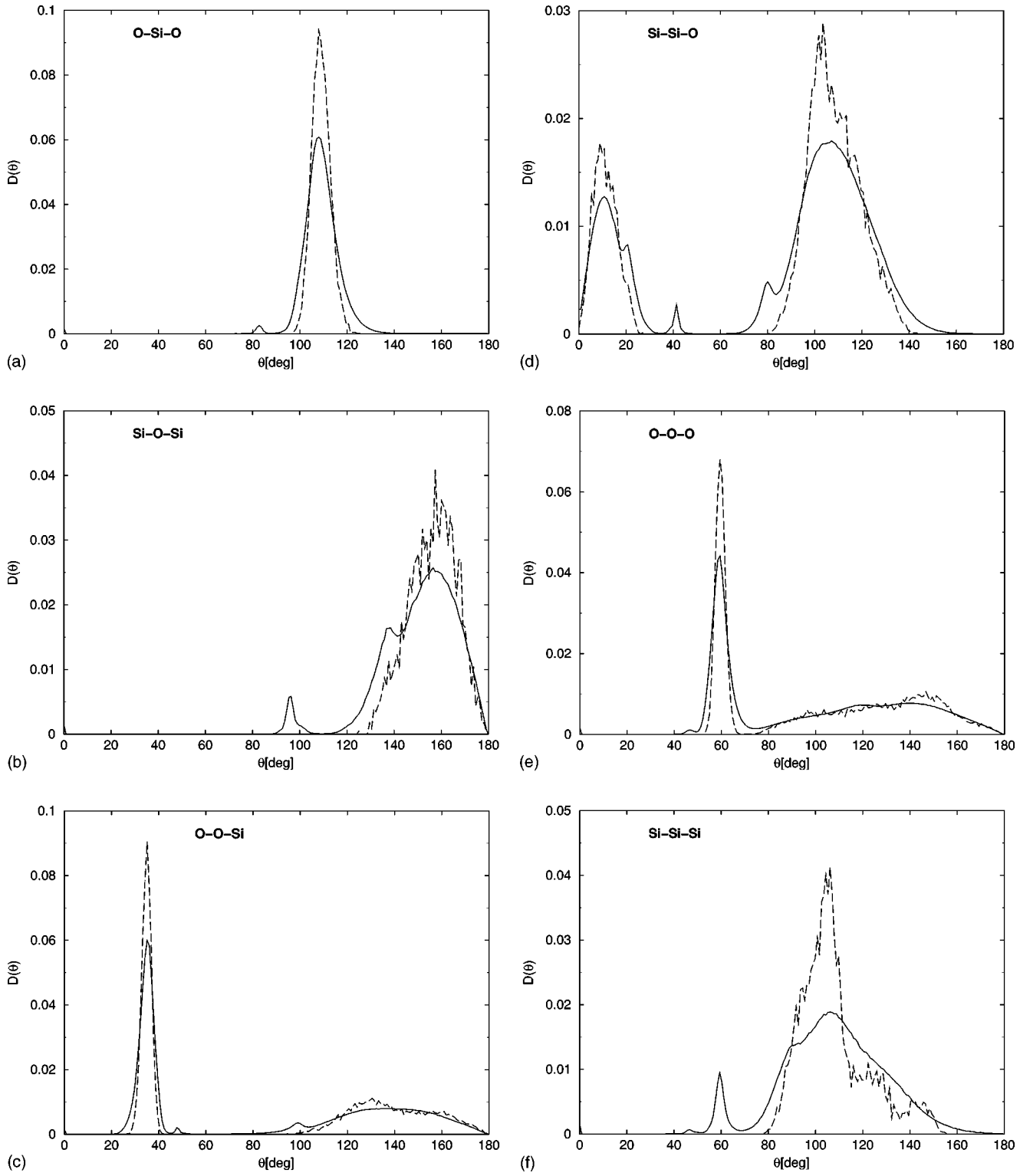

FIG. 2. Bond angle distribution in crystalline ZSM-5 (long-dashed line) and amorphous zeolite derived from ZSM-5 (solid line) at $T = 300$ K. For details refer to Fig. 1

FWHM of 6.2°. These peaks arise from atoms belonging to the same SiO_4 tetrahedra. For an ideal tetrahedron the O-Si-O, O-O-O, and O-O-Si angles are 109.47°, 60°, and 35.26°, respectively. The small deviations from the ideal values show that slightly distorted SiO_4 tetrahedra are the basic structural unit. Besides these peaks other intense peaks related to the connectivity between the SiO_4 tetrahedra are present. Similar to the pair-distribution functions in Fig. 1 smaller peaks at unexpected positions are observed in Fig. 2. All these features will be analyzed in the next section.

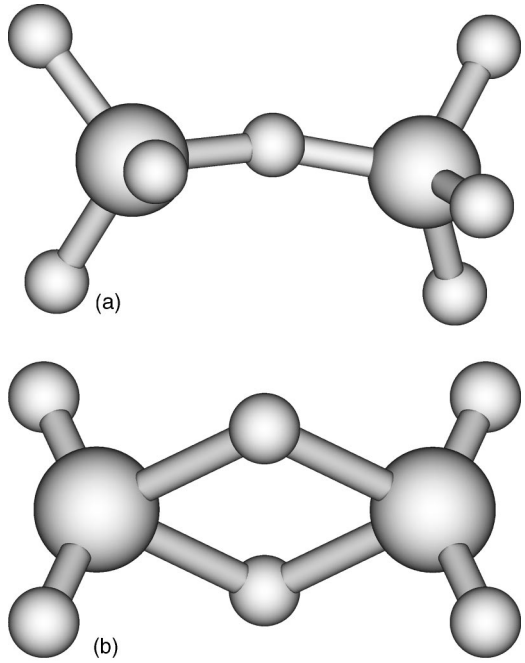

FIG. 3. Model for the connectivity of tetrahedra in amorphous zeolite derived from ZSM-5. (a) Corner-sharing tetrahedra, (b) edge-sharing tetrahedra. (Large spheres represent Si atoms, and small spheres represent O atoms.)

IV. CONNECTIVITY OF THE ELEMENTARY UNITS

Considering the peaks of the pair-distribution and bond angle distribution functions we can interprete that the SiO_4 tetrahedra are linked in two ways as shown in Fig. 3. The model shown in Fig. 3(a) corresponds to the usual corner-sharing tetrahedra network. This structural pattern can be inferred from the peak of the Si-O-Si angle distribution at 157° with a broad FWHM of 40°, which represents the connectivity between two Si atoms present in neighboring tetrahedra with corner sharing. The broad Si-O-Si angle distribution in the amorphous phase compared to the one obtained in the crystal indicates a considerable amount of flexibility in the Si-O-Si angle which is a major source of the disorder and allows for relaxation in a strained system. It has even been shown by the ball-milling experiments of Kosanovic *et al.*[16] that breaking of these Si-O-Si bonds occurs in high silica zeolites and results in the collapse of the crystal structure, leading to the formation of the amorphous phase. In the Si-Si-O angle distribution the peak around 21° comes from two silicon atoms bound to the same oxygen. The broad distribution from 80° to 180° in the O-O-O angle stems from O atoms bound to different Si atoms. The bond angle distribution for Si-Si-Si is peaked at 59°, stemming mainly from Si atoms at their nearest-neighbor distance of ≈ 3 Å, and exhibits a broad maximum at 106°, hinting at a pattern in which Si is distorted, tetrahedrally surrounded by four Si atoms at ≈ 5 Å. The first peaks point to the existence of threefold rings in this ZSM-5 based amorphous form, whereas the broad maximum results from the usual coordination between SiO_4 tetrahedra also present in the crystal.

The positions of the first and less intense peaks in $g_{0\text{-}0}$ and $g_{Si\text{-}Si}$ occurring around 2.2 Å and 2.5 Å, respectively, look surprising at first glance. But selectively collecting the coordinates of such configurations provides strong evidence for the presence of edge-sharing SiO_4 tetrahedra. These are present in small percentages of around 1%–4% (depending on the extent of amorphization) in the ensemble of collected configurations. This model of edge sharing between tetrahedra, as shown in Fig. 3(b), is also in agreement with the small peaks appearing in the bond angle distributions of O-Si-O at 83°, Si-O-Si at 95°, O-O-Si at 48°, and Si-Si-O at 42°. These are related to four atoms, i.e., the Si centers of two edge-shared tetrahedra as well as the bridging O atoms. The peak at 83° in the O-Si-O bond angle distribution shows that the edge-shared tetrahedra are distorted severely. Edge-sharing tetrahedra are also found in nature in the SiO_2 allotrope W-silica[31] and the silicate mineral leucophoenicite $Mn_7(SiO_4)_3(OH)_2$.[32] We note that in Car-Parrinello molecular dynamics studies of dehydroxylated silica surface also edge-shared tetrahedra are observed.[33] However, the edge-shared tetrahedral structures in nature are quite rare, which is usually explained by Pauling's third rule in terms of Coulombic repulsion between the cations sharing polyhedral units. Pauling's third rule states that the presence of shared edges and especially of shared faces in a coordinated structure decreases its stability. Violation of the rule is strong evidence that the structure is covalent.

In the past molecular orbital studies at the SCF-Xα and CNDO/2 levels of the rhombohedral molecule Si_2O_2 and two silicate tetrahedra sharing a common edge and saturated with hydrogens at the periphery, i.e., $Si_2O_6H_4$, have shown that covalent forces play an important role in causing edge-sharing-type distortions.[34,35] In order to analyze the validity of the results for such structural units obtained via MD, we carried out geometry optimizations using gradient-corrected density functional theory (DFT), Hartree-Fock theory (HF), and Møller-Plesset perturbation theory to second order (MP2) on the edge-shared model system $Si_2O_6H_4$. The DFT and MP2 calculations were performed using the TURBOMOLE (Ref. 36) and MOLPRO (Refs. 37 and 38) program packages, respectively. Geometric parameters for the bridged unit for edge-shared tetrahedra are presented in Table I. It is obvious that the result of MD for the amorphous form derived from ZSM-5 is consistent with the experimental data for W-silica and the quantum chemical values for the edge-sharing model system. Note that the DFT and MP2 calculations on the model system do not include the effect of the surroundings. Frequency calculations at the HF level on the edge-shared model system give all positive frequencies, indicating that the structure corresponds to a local minimum. In the polarized Raman spectra of vitreous SiO_2, the D_1 defect line at 495 cm^{-1} was left unassigned.[45,46] We suggest that this could be due to the out-of-plane bending motion of the bridged unit, which was obtained in our frequency calculation on the edge-shared model system at 510 cm^{-1}. It is fair to note, however, that other interpretations also exist; i.e., no edge-sharing tetrahedra were observed in the Car-Parrinello dynamics of vitreous silica and the D_1 defect line was associated with a breathing motion of threefold rings.[47]

TABLE I. Bond distances R (in Å) and bond angles ϕ (in degrees) for the bridged unit in edge-shared SiO_4 tetrahedra. For the sake of comparison the experimental result on W-silica from Ref. 31 is provided.

	Expt.	MD	DFT				MP2
			BP86 [a]		B3LYP [b]		
			TZVP [c]	TZVPP [d]	TZVP [c]	TZVPP [d]	aug-cc-p-vtz [e]
$R_{Si\text{-}Si}$	2.58	2.45±0.1	2.39	2.37	2.39	2.37	2.38
$R_{O\text{-}O}$	-	2.16±0.05	2.41	2.40	2.38	2.37	2.37
$R_{Si\text{-}O}$	1.87±0.09	1.7±0.16	1.70	1.69	1.69	1.68	1.68
$\phi_{O\text{-}Si\text{-}O}$	-	83°	90.4°	90.7°	89.6°	90.0°	89.6°
$\phi_{Si\text{-}O\text{-}Si}$	-	95°	89.6°	89.3°	90.4°	90.0°	90.4°

[a]Becke's gradient-corrected exchange functional (Ref. 39) in combination with Perdew's correlation functional (Ref. 40).

[b]Becke's hybrid three-parameter exchange functional (Ref. 41) with nonlocal correlation provided by Lee, Yang, and Parr (Ref. 42).

[c]Valence triple-ζ basis set with one polarization function.

[d]Valence triple-ζ basis set with two polarization functions.

[e]Augmented correlation-consistent polarized valence triple-ζ basis set of Dunning (Refs. 43 and 44).

V. EXTENT OF AMORPHIZATION

It was shown recently that there is a direct connection between the percentage of crystallinity of partially crystalline zeolitic material and its catalytic properties and ion exchange capacity.[13,11,48] If such chemical properties are based mainly on electronic effects, accurate quantum chemical calculations are needed for their investigation and explanation. However, in zeolitic systems steric effects play a great role to direct selectivities of reactions. These can be investigated by analysis of structures obtained by MD. Hence we choose a semiquantitative description to analyze the extent of amorphization, which is similar to the percentage of XRD crystallinity advocated by Nicolaides.[11] In order to get a measure independent of the number of atoms in the central MD box we choose the energy per atom as a criterion to describe the extent of amorphization of the system. We define the ''percentage of energy crystallinity'' (PEC), i.e.,

$$PEC = \frac{E_{amorphous} - E_{configuration}}{E_{amorphous} - E_{crystalline}} \times 100, \qquad (5)$$

as a normalized dimensionless measure of the extent of amorphization. Here $E_{amorphous}$ corresponds to the energy per atom of the maximum amorphized structure we have obtained after minimization in our simulation, i.e., -16.90 eV/atom (in the part of configurational space spanned in our simulation no higher-lying minimum occurs), and $E_{crystalline}$ corresponds to the energy per atom of the crystalline ZSM-5 system, i.e., -17.17 eV/atom. $E_{configuration}$ stands for the energy of the structure whose PEC we are interested in. It should be mentioned that clearly our definition of PEC depends on the maximum extent of amorphization obtained in the simulations, i.e., on the maximum temperature (here 5000 K) as well as the quenching rate (here 4.7×10^{12} K/s).

As shown in Fig. 4, the comparison between the cross section of crystalline ZSM-5 and the simulated ZSM-5 based amorphous structure, the amorphization leads to local disorder and partial collapse of the framework structure. It is mainly this modification of pores and cavities which may allow a tuning of properties of significant interest. In Fig. 5 the distribution of coordination numbers (Z) for O atoms (Z_O) and Si atoms (Z_{Si}) for different PEC is given. If the interatomic distance $r<1.8$ Å [i.e., the distances corresponding to the first peak in the pair-distribution function, Fig. 1(a)], then the atoms are considered to be neighbors. One can easily observe the fraction of coordination defects; i.e., atoms with coordination numbers other than the ideal ones ($Z_O=2$ and $Z_{Si}=4$) decrease with PEC. Even in highly amorphized structures (low PEC) 95% of O atoms and 90% of Si atoms remain twofold and fourfold coordinated, respectively. Only 3% of the O atoms are undercoordinated ($Z_O=1$) and 2% overcoordinated ($Z_O=3$). In the case of the Si atoms around 9% are undercoordinated ($Z_{Si}=3$) and 1% overcoordinated ($Z_{Si}=5$). The analysis by linear regression suggests that in this amorphous material low coordinations are more favored than high coordinations; cf. Fig. 5. We note that also in other related amorphous systems, e.g., SiO_2 glass at low temperature,[49] undercoordination of Si and O is preferred, whereas with increasing temperature overcoordination of both Si and O becomes more frequent.[49,50] However, in the molecular dynamics simulation of silica glasses it was shown by Feuston and Garofalini that the coordination number distribution strongly depends on the interaction potential used and that the structures obtained by the introduction of three-body potentials have fewer defects compared to those derived from calculations using only pair potentials.[51]

Among the most characteristic structural features of zeolites are their large internal surface area (ISA) and high porosity, which both are important factors for catalytic properties (apart from the presence of acidic sites in heteroatom-substituted zeolites). Therefore it is of interest to study the dependence of both the ISA and porosity on the degree of amorphization, e.g., the PEC. In order to calculate the ISA we model the system as an ensemble of intersecting hard spheres with radii depending on the CN of the constituting

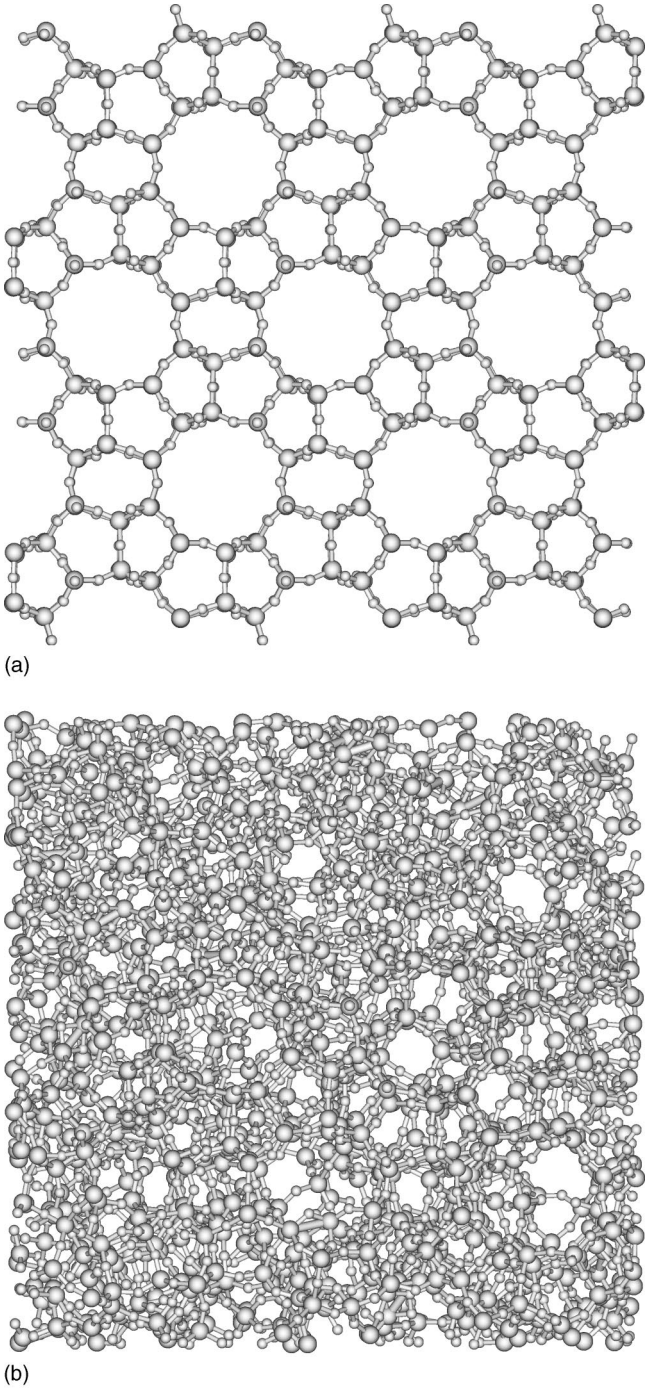

FIG. 4. Cross section of (a) ZSM-5 (crystalline), (b) simulated amorphous form derived from ZSM-5 with 60% crystallinity. Large and small spheres represent Si and O atoms, respectively. In both figures 3456 atoms are displayed and the view is along the *Y* axis.

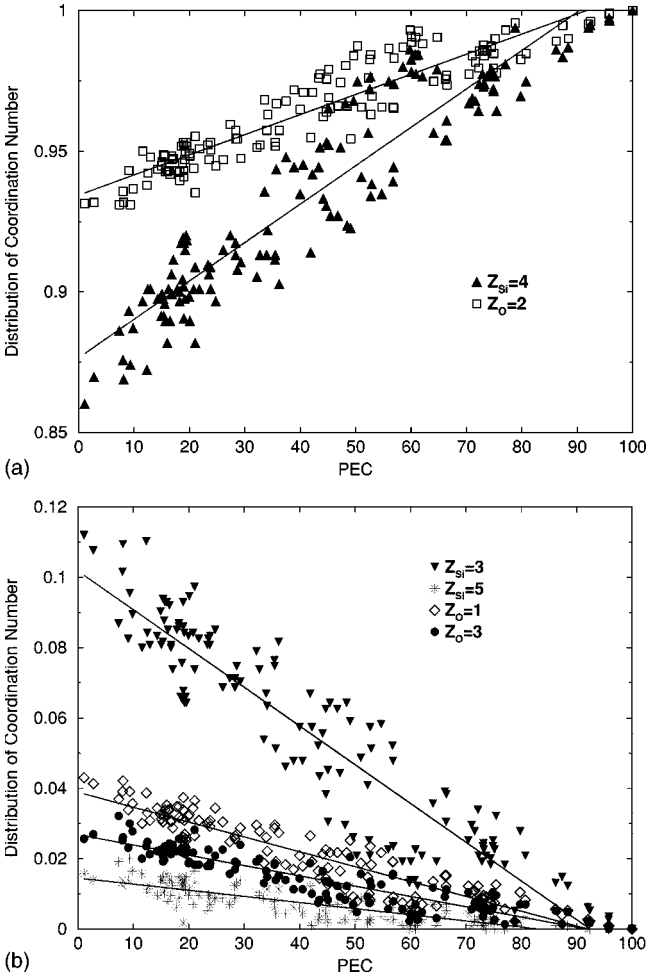

FIG. 5. (a) Distribution of coordination numbers in which an O atom is surrounded by two atoms ($Z_O=2$) and a Si atom is surrounded by four atoms ($Z_{Si}=4$) vs percentage of energy crystallinity (PEC). (b) Distribution of coordination number in which an O atom is surrounded by one atom ($Z_O=1$) and three atoms ($Z_O=3$) and a Si atom is surrounded by three atoms ($Z_{Si}=3$) and five atoms ($Z_{Si}=5$). The solid lines were obtained from linear regression and should serve as guides for the eye, for each distribution. Note the difference in scale of the *y* axis in (a) and (b). The data displayed result from a total of 140 configurations.

atoms/ions. The CN of Si/O was determined as the number of O/Si centers within a distance of 1.8 Å; i.e., all bonds contributing to the first peak in the pair-distribution function $g_{Si\text{-}O}$ [Fig. 1(b)] were included. Since the higher the CN of an atom and ion in the framework, the lower its contribution to the ISA, we chose the radii according to Table II: for uncoordinated atoms the van der Waals radii were chosen,[52] whereas for standard CN four for Si and two for O the ionic radii of Si^{4+} and O^{2-} were selected.[53] For intermediate values of the CN a linear interpolation was used. Contributions of atoms and ions with higher than the standard CN were neglected.

The effective ISA of the system under study depends also on the size of the probe used to measure it. A standard way to derive the effective ISA is the so-called probe-atom model, where the ISA is defined by a surface generated by the center of a hard test sphere of radius r_{probe} rolling over the ensemble of intersecting spheres.[52] Recently Moloy *et al.* demonstrated for various crystalline zeolites that the ISA decreases by a factor of 1.4–2.8 when the radius of the probe atom is increased from 0.5 Å to 1.1 Å.[54] We therefore applied four different radii of the probe atom, i.e., 0.5, 1.0, 1.5, and 2.0 Å, in order to investigate the probe size dependence

TABLE II. Atomic/ionic radii R_{coord} (in Å) for O and Si depending on the coordination number (CN).

CN	R_{coord} (O)	R_{coord} (Si)
0	1.52 [a]	2.10 [b]
1	1.435	1.64
2	1.35 [c]	1.18
3	0	0.72
4	0	0.26 [d]
5 and higher	0	0

[a]Van der Waals radius of the O atom.
[b]Van der Waals radius of the Si atom.
[c]Ionic radius of O^{2-} having CN 2.
[d]Ionic radius of Si^{4+} having CN 4.

of the ISA upon amorphization. For practical calculations of the ISA we incremented the radii of the intersecting spheres described above by the probe-atom radius. The surface of the resulting ensemble of sphere was estimated as

$$\mathrm{ISA} = \frac{1}{M}\left(\sum_{i=1}^{N} 4\pi [R_{coord}(i) + r_{probe}]^2 \frac{p_i}{p} \right). \qquad (6)$$

Here the sum runs over all N centers i in the MD box, $R_{coord}(i)$ refers to the atom-ion radius from Table II, r_{probe} is the probe-atom radius, and M refers to the amount of SiO_2 present in the structure considered. A total of p points (here $p=614$) is distributed equally on the surface of each sphere i, and the number p_i of points not located inside other spheres is determined. The ratio p_i/p then provides the fraction of the accessible surface contributed by center i. Note that our definition of the ISA does not consider cases where there may be internal surfaces which are not accessible due to the abscence of windows by which probe molecules can enter. Therefore, the values obtained here represent upper bounds to the actual accessible internal surface area.

Figures 6(a)–6(d) contain our result for the ISA of 310 configurations determined with four different probe radii. Our values for crystalline ZSM-5, i.e., 160.77 and 83.86 $m^2 \times 10^3$/mol for probe-atom radii of 0.5 and 1.0 Å, respec-

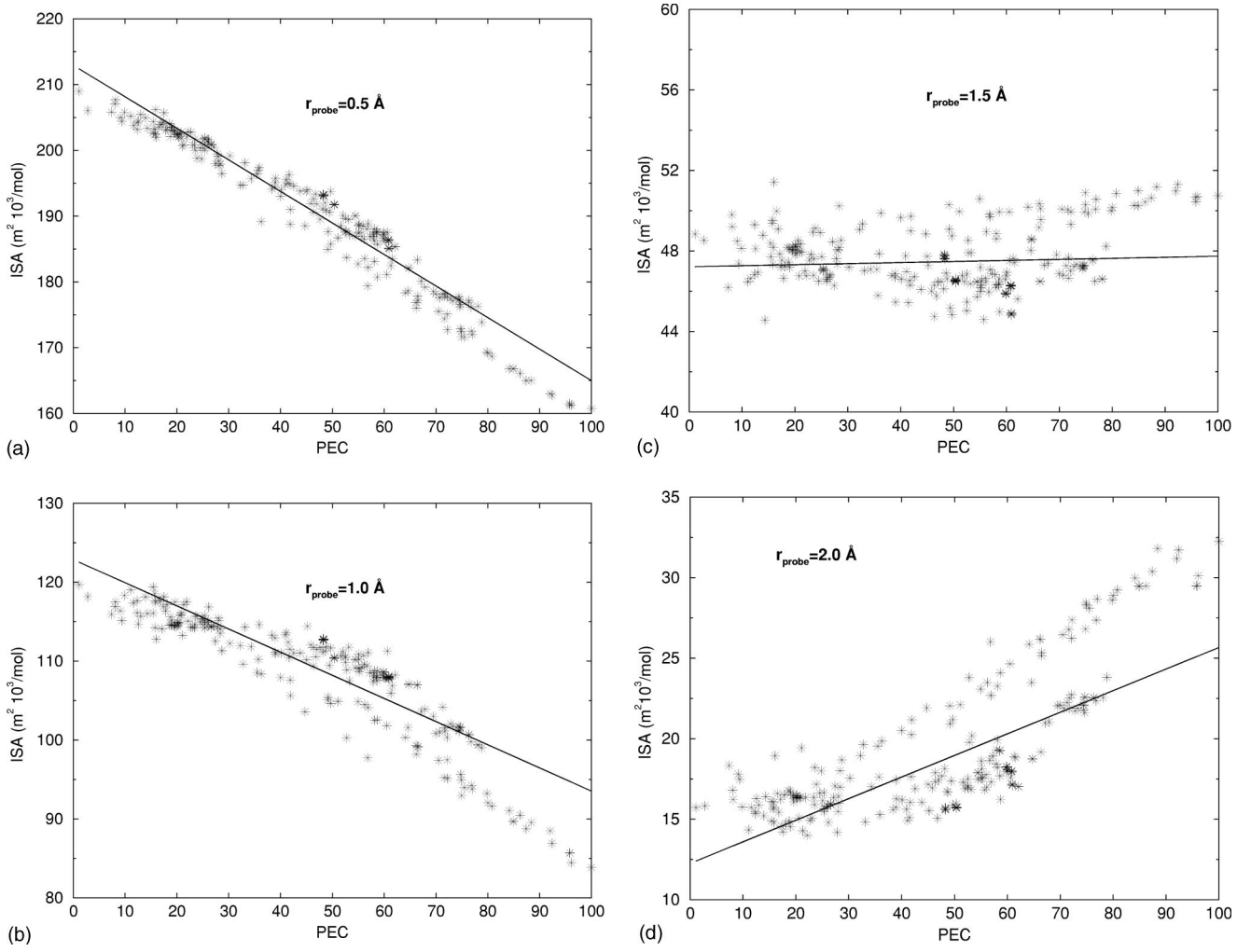

FIG. 6. Internal surface area (ISA) vs percentage of energy crystallinity (PEC) for 310 configurations in dependence of the probe-atom radius. The straight lines are taken from a linear regression (slopes= −0.479, −0.293, 0.005, 0.134, intercept= 212.94, 122.87, 47.20, 12.26 in units of the plot for r_{probe}=0.5 Å, 1.0 Å, 1.5 Å, 2.0 Å).

TABLE III. Ring analysis for ZSM-5 based amorphous material depending on the extent of amorphization at 300 K measured as percentage of energy crystallinity (PEC). The first line for each PEC gives the occurence of *n*-fold rings in percent (%). In the second and third lines the average and minimal radii $\overline{r}_{avg}$ and $\overline{r}_{min}$ are listed (in Å). The rightmost column contains estimate of the pore size S_{avg} and S_{min}.

PEC	$n=2$	3	4	5	6	7	8	9	10	Pore size
100	-	-	2.9	48.9	39.2	-	-	-	9.0	
			2.19	2.57	2.85				4.70	2.86
			2.16	2.42	2.53				4.32	2.62
79	1.0	2.6	9.0	37.7	33.4	8.2	2.4	1.9	3.8	
	1.22	1.72	2.17	2.58	2.89	3.28	3.65	4.16	4.68	2.81
	1.22	1.66	2.04	2.37	2.50	2.70	2.97	3.49	4.17	2.48
60	2.5	7.5	13.2	20.9	35.0	15.0	3.6	1.3	1.0	
	1.23	1.71	2.16	2.54	2.68	3.29	3.70	4.06	4.49	2.64
	1.23	1.66	2.01	2.26	1.87	2.70	3.00	3.04	3.54	2.13
45	3.7	8.0	15.3	28.5	26.7	12.1	2.9	2.2	0.7	
	1.23	1.88	2.50	3.07	2.78	3.29	3.63	4.01	4.26	2.82
	1.23	1.64	2.00	2.19	1.94	2.67	2.84	3.08	2.99	2.12
15	4.0	13.0	17.3	29.3	26.8	5.7	2.0	1.3	0.6	
	1.25	1.90	2.54	3.00	2.57	3.22	3.42	3.80	4.12	2.63
	1.25	1.57	1.81	1.81	1.37	2.52	2.58	2.29	2.44	1.71

tively, are in excellent agreement with results published by Moloy *et al.*, i.e., ≈ 162 and ≈ 84 $m^2 \times 10^3$/mol (taken from their Fig. 7, entry MFI).[54] Amorphization leads to a collapse of the zeolitic framework and reduces the number of large pores (cf. also the discussion of ring statistics given below). This is evident from Fig. 6 for $r_{probe}=2.0$ Å, where amorphization decreases the ISA by roughly a factor of 2. However, for a small probe radius such as $r_{probe}=0.5$ Å one observes an increase of the ISA by about a factor of 2. This is explained partly by the increasing percentage of undercoordinated centers in the amorphous system (cf. Fig. 5), but also by the increasing tendency to convert larger rings into smaller rings (cf. below). In conclusion amorphization makes the framework less accessible for larger species and more accessible for smaller ones. Such structural changes can be of high importance for catalysis, where the accessibility of the acidic sites (in the case of protonated ZSM-5) and the rate of adduct-product exchange at the active site can be the crucial parameters to influence the yield and selectivity of certain reactions.[48,55] Changes in the network topology may also result in the closure of sites suitable for ion exchange (in case of hetero-atom substituted zeolites).

In order to gain further insight into the connectivity between the SiO_4 tetrahedra and to measure quantitatively the effects of amorphization on the structure, e.g., the porosity, we performed a ring analysis. In the following we define a *n*-fold ring by the number *n* of Si atoms connected by bridging O to give a ring. The number of Si atoms was determined by first assigning to each bridging O atom a pair of adjacent Si atoms and then tracing possible connections to a ring containing a maximum of up to 15 Si atoms. Double counting is avoided and sets of Si atoms defining a small ring are not allowed to contribute as a whole to a large ring. Since rings can extend to periodic images of the MD boxes, the periodic boundary condition was removed for determining the ring distribution. The latter is sensitive to the temperature and the threshold for the maximum distance between bonded atoms; thus configurations with similar PEC can exhibit slight differences in their ring distributions. The statistics for *n*-fold rings presented in Table III nevertheless clearly shows characteristic features depending on the PEC.

Crystalline ZSM-5 contains mainly fivefold (48.9%) and sixfold (39.2%) rings, along with a smaller amount of tenfold (9.0%) and fourfold (2.9%) rings. Amorphization is found to lead to a broad distribution of ring sizes from 2 to 10. In 15% energy crystalline amorphous material we observe still fivefold (29.3%) and sixfold (26.8%) rings to be most frequent; however, also fourfold (17.3%) and threefold (13.0%) rings contribute significantly. We can compare these findings to those from previous related work on SiO_2 glass, which exhibits a pronounced dominance of sixfold rings; i.e., threefold to sixfold rings contribute with 3.0%, 11.1%, 24.2%, and 61.6%, respectively.[56] Whereas for our system at small PEC (as well as for the crystal) larger than sixfold rings are present to less than 10%, they contribute with up to 20% for intermediate values of PEC. In these cases sevenfold rings contribute roughly as much as fourfold ones. Therefore, besides the collapse of the tenfold rings in crystalline ZSM-5 upon amorphization, also a ''fusion'' of smaller membered rings to more than sixfold rings must occur.

The bond angle distributions suggest that both twofold and threefold rings are essentially planar. For twofold rings Si-O-Si and O-Si-O angle distributions have a peak near 90° and for threefold rings Si-Si-Si and O-O-O angle distributions have a peak near 60°. This result agrees quite well with the finding of Galeener based on force-field calculations that twofold and threefold rings of Si-O bonds in the vitreous form of SiO_2 are expected to be planar.[46] The presence of twofold rings again indicates the existence of edge-sharing

tetrahedra. However, the modest number of twofold rings suggests that most tetrahedra are linked to each other by corners.

Much more difficult than the purely topological analysis of ring sizes is their geometrical measurement. Whereas small rings are essentially planar, larger ones are usually puckered considerably and make the definition of a ring diameter meaningless. Therefore, we calculate two simple measures for each ring, i.e.,

$$r_{avg}=\frac{1}{n}\sum_{\substack{i=1\\ i\in ring}}^{n}|\boldsymbol{R}_{Si}(i)-\boldsymbol{R}_c| \tag{7}$$

and

$$r_{min}=\min_{i\in \text{ring}}|\boldsymbol{R}_{Si}(i)-\boldsymbol{R}_c|. \tag{8}$$

The center of an n-fold ring $\boldsymbol{R}_c$ herein is defined as

$$\boldsymbol{R}_c=\frac{1}{n}\sum_{\substack{i=1\\ i\in ring}}^{n}\boldsymbol{R}_{Si}(i). \tag{9}$$

The quantity r_{min} gives a maximum radius below which atoms and molecules will be able to pass through the ring. For planar and regular rings r_{min} will be close to the average r_{avg}; for puckered and irregular rings r_{avg} will be significantly larger than r_{min}. Measures $\overline{r}_{avg}$ and $\overline{r}_{min}$ for the effective size of a certain type of rings are then generated by averaging r_{avg} and r_{min} over all rings of the specific type in the systems. Clearly, these quantities derived solely from the positions of the Si atoms are to a certain extent arbitary. In reality the effective ring size depends not only on the electron density distribution of the Si and O atoms in the ring but also on the one of the probe system. In addition vibrational motion will affect the effective ring size. Summing up, a well-defined unique probe-independent measure of ring size cannot be given; nevertheless, we believe that the values of $\overline{r}_{avg}$ and $\overline{r}_{min}$ listed also in Table III provide reasonable trends.

For crystalline ZSM-5 the values of $\overline{r}_{avg}$ and $\overline{r}_{min}$ are quite similar with a maximum deviation of $\approx$13% for sixfold rings. With increasing degree of amorphization the ratio $\overline{r}_{avg}/\overline{r}_{min}$ increases up to almost a factor of 2 for some ring sizes, i.e., $\approx$1.9 for sixfold and $\approx$1.7 for fivefold, ninefold, and tenfold rings. This indicates that the most frequently occurring ring types (fivefold and sixfold) have the largest tendency to irregular shape and puckering, leading to smaller effective pore sizes in amorphous systems.

From the individual ring averages $\overline{r}_{avg}$ and $\overline{r}_{min}$ we can derive global averages S_{avg} and S_{min} for the amorphous system (cf. the right column in Table III) by weighting the ring-specific values $\overline{r}_{avg}$ and $\overline{r}_{min}$ with the occurrence of the ring types. These should have some relation to measured effective pore sizes. Whereas the averaged value S_{avg} does not exhibit a clear trend with decreasing PEC, the average S_{min} clearly decreases. This finding is in line with the concomittant decrease of ISA for large probe atoms depicted in Fig. 6. We conclude that S_{min} might be more helpful in a discussion of catalytic processes. Finally we want to mention that despite all reservations the order of magnitude of S_{min} appears to be realistic: for crystalline ZSM-5 we estimate an effective pore diameter of at least 5.2 Å. This agrees well with the value of around 5.5 Å of the micropore size distribution by Saito and Foley obtained experimentally from high resolution argon adsorption on ZSM-5.[57]

VI. CONCLUSION AND FUTURE DIRECTIONS

In the present paper we have investigated the structural properties of ZSM-5 based amorphous material by means of a molecular dynamics technique by using transferable potentials. Our simulations gave a detailed account of many significant stuctural properties at the microscopic level which explain the modified properties and applications of these low crystalline and amorphous materials. The simulations showed that the elementary building blocks are distorted SiO_4 tetrahedra which are mainly connected by corner sharing. A small percentage of edge-shared tetrahedra are also present in the simulated structures. Two-body structural correlation was analyzed by pair-distribution functions and showed the average bond distance between Si and O atoms to be about 1.62 Å. Si-Si and O-O distances correspond to 3.19 Å and 2.61 Å, respectively. Three-body structural correlation was analyzed by bond angle distributions and supports the presence of mainly corner sharing tetrahedra in the network along with a small percentage of edge-sharing ones. The extent of amorphization was quantified by the parameter ''percentage of energy crystallinity.'' Crucial properties like coordination number distribution, effective internal surface area, ring size distribution, and effective pore size are found to be a functional of the extent of amorphization. Amorphization leads to a collapse of the framework which reduces for large species the porosity of the system and brings about a closure of large-sized rings and channels. Whereas for larger species the effective internal surface is reduced by this process, it is increased for smaller species, probably due to the increase of the amount of undercoordinated atoms and the generation of smaller rings from larger ones. Hence, it can affect properties like ion exchange and steric effects on reactions. In the amorphous phase fivefold and sixfolds rings contribute most to the ring distribution followed by fourfold, threefold, and sevenfold rings; however, due to irregular ring shape, the pores provided by fivefold and especially sixfold rings appear to be relatively small.

The present work focused on the structural aspects of the ZSM-5 based amorphous system, whereas an upcoming publication will deal with its dynamical properties (vibration and relaxation).[30]

ACKNOWLEDGMENT

Funding by the Deutsche Forschungsgemeinschaft through the SFB408 is gratefully acknowledged.

*Electronic address: basu@thch.uni-bonn.de

[1] A. Corma, Chem. Rev. **95**, 559 (1995).
[2] P. B. Venuto, Microporous Mater. **2**, 297 (1994).
[3] P. B. Venuto, Stud. Surf. Sci. Catal. **105**, 811 (1997).
[4] J. E. Naber, K. P. de Jong, W. H. J. Stork, H. P. C. E. Kuipers, and M. F. M. Post, Stud. Surf. Sci. Catal. **84**, 2197 (1994).
[5] W. O. Haag, Stud. Surf. Sci. Catal. **84**, 1375 (1994).
[6] A. Moirou, A. Vaxevanidou, G. E. Christidis, and I. Paspaliaris, Clays Clay Miner. **48**, 563 (2000).
[7] J. S. Kim, L. Zhang, and M. A. Keane, Sep. Sci. Technol. **36**, 1509 (2001).
[8] P. Misaelides and A. Godelitsas, Czech. J. Phys. **49**, 167 (1999).
[9] J. P. Ackerman, L. S. H. Chow, S. M. McDeavitt, C. Pereira, and R. H. Woodman, JOM-J. Min. Met. Mat. Soc. **49**, 26 (1997).
[10] S. Mintova, B. Schoeman, V. Valtchev, J. Sterte, S. Y. Mo, and T. Bein, Adv. Mater. **9**, 585 (1997).
[11] C. P. Nicolaides, Appl. Catal., A **185**, 211 (1999).
[12] S. X. Wang, L. M. Wang, and R. C. Ewing, J. Nucl. Mater. **278**, 233 (2000).
[13] B. X. Gu, L. M. Wang, and R. C. Ewing, J. Nucl. Mater. **278**, 64 (2000).
[14] R. A. Secco and Y. Huang, J. Phys. Chem. Solids **60**, 999 (1999).
[15] C. Kosanovic, B. Subotic, and I. Smit, Thermochim. Acta **317**, 25 (1998).
[16] C. Kosanovic, A. Cizmek, B. Subotic, I. Smit, M. Stubicar, and A. Tonejc, Zeolites **15**, 51 (1995).
[17] C. Kosanovic and B. Subotic, Microporous Mater. **12**, 261 (1997).
[18] A. B. Mukhopadhyay (unpublished).
[19] C. Oligschleger and B. B. Laird (unpublished).
[20] G. J. Kramer, N. P. Farragher, B. W. H. van Beest, and R. A. van Santen, Phys. Rev. B **43**, 5068 (1991).
[21] G. J. Kramer, A. J. M. de Man, and R. A. van Santen, J. Am. Chem. Soc. **113**, 6435 (1991).
[22] S. W. de Leeuw, J. W. Perram, and E. R. Smith, Proc. R. Soc. London, Ser. A **373**, 27 (1980).
[23] D. H. Olson, G. T. Kokotailo, S. L. Lawton, and W. M. Meier, J. Phys. Chem. **85**, 2238 (1981).
[24] K. Vollmayr, W. Kob, and K. Binder, J. Chem. Phys. **105**, 4714 (1996).
[25] K. Vollmayr, W. Kob, and K. Binder, Phys. Rev. B **54**, 15 808 (1996).
[26] L. V. Woodcock, Chem. Phys. Lett. **10**, 257 (1971).
[27] H. J. C. Berendsen and J. Postma, J. Chem. Phys. **72**, 2384 (1980).
[28] G. J. Martyna, M. L. Klein, and M. Tuckerman, J. Chem. Phys. **97**, 2635 (1992).
[29] R. Fletcher and C. M. Reeves, Comput. J. (UK) **7**, 149 (1964).
[30] A. B. Mukhopadhyay, C. Oligschleger, and M. Dolg (unpublished).
[31] V. A. Weiss and A. Weiss, Z. Anorg. Allg. Chem. **276**, 95 (1954).
[32] P. B. Moore, Am. Mineral. **55**, 1146 (1970).
[33] D. Ceresoli, M. Bernasconi, S. Iarlori, M. Parrinello, and E. Tosatti, Phys. Rev. Lett. **84**, 3887 (2000).
[34] J. A. Tossell and G. V. Gibbs, Am. Mineral. **61**, 287 (1976).
[35] J. A. Tossell and G. V. Gibbs, J. Mol. Struct. **35**, 273 (1976).
[36] R. Ahlrichs, M. Bär, M. Häser, H. Horn, and C. Kölmel, Chem. Phys. Lett. **162**, 165 (1989).
[37] H.-J. Werner and P. J. Knowles, MOLPRO ab initio electronic structure package, version 2000.1, 2000.
[38] C. Hampel, K. Peterson, and H.-J. Werner, Chem. Phys. Lett. **190**, 1 (1992).
[39] A. D. Becke, Phys. Rev. A **38**, 3098 (1988).
[40] J. P. Perdew, Phys. Rev. B **33**, 8822 (1986).
[41] A. D. Becke, J. Chem. Phys. **98**, 5648 (1993).
[42] C. Lee, W. Yang, and R. G. Parr, Phys. Rev. B **37**, 785 (1988).
[43] T. Dunning, J. Chem. Phys. **90**, 1007 (1989).
[44] D. E. Woon and T. Dunning, J. Chem. Phys. **98**, 1358 (1993).
[45] F. L. Galeener and G. Lucovsky, Phys. Rev. Lett. **37**, 1474 (1976).
[46] F. L. Galeener, J. Non-Cryst. Solids **49**, 53 (1982).
[47] A. Pasquarello and R. Car, Phys. Rev. Lett. **80**, 5145 (1998).
[48] C. P. Nicolaides, H. H. Kung, N. P. Makgoba, N. P. Sincadu, and M. S. Scurrell, Appl. Catal., A **223**, 29 (2002).
[49] C. Oligschleger, Phys. Rev. B **60**, 3182 (1999).
[50] J. Horbach and W. Kob, Phys. Rev. B **60**, 3169 (1999).
[51] B. P. Feuston and S. H. Garofalini, J. Chem. Phys. **89**, 5818 (1988).
[52] C. Accelrys Inc., San Diego, CERIUS^2 modeling software, 2001, eprinthttp://www.msi.com/cerius2.
[53] *CRC Handbook of Chemistry and Physics*, edited by R. C. Weast (CRC Press, Cleveland, OH, 2000).
[54] E. C. Moloy, L. P. Davila, J. F. Shackelford, and A. Navrotsky, Microporous Mesoporous Mater. **54**, 1 (2002).
[55] J. Xie and S. Kaliaguine, Appl. Catal., A **148**, 415 (1997).
[56] T. F. Soules, J. Chem. Phys. **71**, 4570 (1979).
[57] A. Saito and H. C. Foley, Microporous Mater. **3**, 543 (1995).